Desalination and Water Treatment
www.deswater.com

doi: 10.5004/dwt.2019.24352

162 (2019) 290–302
September

Brief study on the kinetic aspect of photodegradation of sulfasalazine aqueous solution by cuprous oxide/cadmium sulfide nanoparticles

Narges Omrani[a,b], Alireza Nezamzadeh-Ejhieh[a,b,c,*], Mohammad Alizadeh[b,c]

[a]*Department of Chemistry, Shahreza Branch, Islamic Azad University, P.O. Box 311-86145, Shahreza, Isfahan, Iran, emails: arnezamzadeh@iaush.ac.ir (A. Nezamzadeh-Ejhieh), omraninarsis@yahoo.com (N. Omrani)*
[b]*Young Researchers and Elite Club, Shahreza Branch, Islamic Azad University, Shahreza, Iran, Tel. +98 31-53292500; email: alizadeh1449@yahoo.com*
[c]*Razi Chemistry Research Center (RCRC), Shahreza Branch, Islamic Azad University, Isfahan, Iran*

Received 19 January 2019; Accepted 30 April 2019

ABSTRACT

A boosted photocatalytic activity was obtained for the as-synthesized Cu_2O-CdS nanocomposite (NC) with respect to single Cu_2O and CdS nanoparticles in the photodegradation of sulfasalazine (SFSZ) in aquatic media. X-ray diffraction (XRD) spectroscopy, scanning electron microscope (SEM) and UV–Vis diffuse reflectance spectroscopy were characterization techniques used in this work. The best mole ratio was 2:1 for the Cu_2O/CdS in the composite to achieve the best photodegradation efficiency. After 15 min, 230, 410, 585, 760 and 450 nano-moles of SFSZ molecules were degraded for concentrations of 10, 20, 30, 40 and 50 ppm of SFSZ solutions, respectively. The optimal conditions were CSFSZ: 30 mg L^{-1}, pH 5, 25 min irradiation time and 0.5 g L^{-1} of the Cu_2O-CdS composite. Degradation extents of 94%, 94.7% and 82% were, respectively, estimated for the degradation of SFSZ molecules based on the results obtained by UV–Vis spectroscopy, high-performance liquid chromatography and chemical oxygen demand measurements.

Keywords: Kinetic study; Sulfasalazine; Photocatalysis; Cuprous oxide/cadmium sulfide composite

1. Introduction

Nowadays, increased pollution of water by pharmaceutical compounds, especially antibiotics, has impacted the human life in a negative way [1–3]. An antibiotic that is widely used for rheumatoid arthritis treatment is sulfasalazine (SFSZ) with a long life time in environmental waters. Accordingly, it can accumulate in different organisms of the food chain and affect the human health [4,5]. Due to relatively high resistance of such compounds to natural degradation, biodegradation, and photo-transformation, in general, heterogeneous photodegradation has been widely used for destroying of different pollutants in aqueous solutions or gaseous phases. In this technique, the investigated pollutants must be converted to water and carbon dioxide as the final products [6–8].

In general, four reactive species including the photogenerated hole and electrons and also hydroxyl and super oxide radicals are responsible for the degradation of pollutants present in media in a typical heterogeneous semiconducting based photocatalysis process. By irradiation of the subjected semiconductor with an adequate photon (in UV–Vis regions), it can be excited and exit an electron to its conduction band (C_b) and leave a hole in its valence band (V_b). The photogenerated electron–hole (e/h) pairs can, respectively, react with dissolved oxygen and water molecules to produce superoxide and hydroxyl radicals, respectively [9–16].

* Corresponding author.

When the photogenerated e/h pairs were recombined, all the used energy can be consumed as heat. This drawback can be overcame by doping, supporting of the semiconductors onto a suitable support, coupling of two or more semiconductors, converting the bulk semiconductor to nano-dimension for reducing the path length for migration of the photogenerated e/h pairs to the surface of the catalyst [17–24].

In the present work, we used the coupling (hybriding, combining) technique to increase the photoactivity of the system. In coupling technique, the internal oxidation/reduction process is responsible for prevention of e/h recombination. Hence, matching of the standard potentials of C_b and V_b levels is very important. Hence, Cu_2O (energy gap: 2.0 eV) and CdS (energy gap: 2.4 eV) semiconductors were selected as the *p*-type and *n*-type semiconductors, respectively [25,26]. In these semiconductors, the standard potentials are as: E^0: Cu_2O-C_b: –1.30 V, CdS-C_b: –0.6 V, Cu_2O-V_b: 0.6 V, CdS-V_b: 1.8 V with respect to NHE [27,28] that are suitable values for coupling them. The resulted composite was then used in photodegradation of SFSZ and kinetics of the process was followed.

2. Experimental

2.1. Reagents and preparations

All analytical grade chemicals including cadmium nitrate, copper(II) acetate, ammonium sulfide, ascorbic acid (AA: $C_6H_8O_6$) etc. used in this work were purchased from Merck or Sigma-Aldrich Co. A 500 mg sulfasalazine pharmaceutical capsule (Iran Daru Co., Iran) was purchased from local drugstores. Distilled water was used for the preparation of solutions/suspensions and wherever pH adjustment was required their pH was adjusted by sodium hydroxide or hydrochloric acid solution.

The following method was used for preparation of cuprous oxide nanoparticles (NPs). 20 mL 0.25 mol L^{-1} NaOH solution was added into a 100 mL 0.27 mol L^{-1} copper(II) acetate solution on a magnetic stirrer (rpm 200) to obtain $Cu(OH)_2$. Then, 15 mL 0.15 mol L^{-1} AA aqueous solution was added (as a reducing agent). After a few minutes, the deep blue color of the solution was appeared and then changed to burgundy type, confirming synthesis of Cu_2O colloid in the presence of dissolved oxygen atmosphere. The suspension was then centrifuged (>13,000 rpm), washed three times with water. The resulted precipitate was then dried at 80°C to obtain Cu_2O NPs [25].

CdS NPs were synthesized by drop wise addition of 100 mL 0.085 mol L^{-1} $Cd(NO_3)_2$ solution to 100 mL 0.1 mol L^{-1} $(NH_4)_2S$ solution under vigorous stirring (1,200 rpm) during 5 h. After centrifugation (>13,000 rpm), the obtained dark yellow CdS NPs were washed with water many times and dried at room temperature [29]. The Cu_2O/CdS composite was prepared by hand mixing of the adequate amount of each component to obtain a required mole ratio in an agate mortar for 10 min.

2.2. Instruments and characterization

XRD pattern of the composite was recorded by an XRD diffractometer model X'PertPro (with Ni-filtered Cu-Kα radiation source at 1.5406 Å, 40 kV, i 30 mA; Netherlands). UV–Vis diffuse reflectance spectrophotometer (JASCO V 670, using $BaSO_4$ as reference, Japan) was used for recording diffuse reflectance spectroscopy (DRS) spectra. FESEM images were recorded by a MIRA3LMU scanning electron microscope (TESCAN Co., Czech Republic). A pH-meter (Jenway model 3505) was used for pH adjustment. A transmission electron microscope (TEM) Philips EM 208s (100 kV) was used for recording the TEM images.

A high-performance liquid chromatography instrument (Agilent Technologies 1200 Series) was used for analysis of SFSZ solutions before and after the photodegradation process (Column: Zorbax@ 5 μm Eclipse-XDB-C_{18} 80 Å; flow rate: 1.0 mL min^{-1}, Mobile phase: A 1:1 mixture of methanol containing 0.1% formic acid and water containing 0.1% formic acid, injection volume: 20 μL, column length: 250 mm, i_d: 4.6 mm, detection wavelength: 345 nm) [5].

2.3. Photodegradation experiments

In the photodegradation experiments, a 10 mL portion of a 10 mg L^{-1} SSZ solution and 0.3 mg L^{-1} Cu_2O-CdS catalyst was added to the 25 mL glass beaker and shaken for 5 min (based on preliminary experiments) to reach equilibrium adsorption/desorption process. After that, the suspension was irradiated by a 40 Tungsten W lamp (Osram electric Co., Iran) which positioned 10 cm above the beaker on a magnetic stirrer (100 rpm). Direct photolysis was also studied at the similar conditions on a solution without the catalyst. Finally, the suspension was centrifuged (>13,000 rpm) at regular times and the absorbance of the cleaned solution was recorded (at λmax = 360 nm for SFSZ). The recorded absorbencies, (A_0 and A, for the samples before and after irradiation process, respectively) were used for the degradation extent of SFSZ (D in %) by using the following equation. According to the Beer–Lambert law, the A_0 and A terms correspond to the initial and final concentrations (C_0 and C, respectively) at time t.

$$D(\%) = \left[\frac{A_0 - A}{A_0}\right] \times 100 = \left[\frac{C_0 - C}{C_0}\right] \times 100 \quad (1)$$

No initial pH adjustment was done except wherever the effect of pH was investigated. Change in initial pH of solutions during the photodegradation process as the function of some pivotal investigated parameters are summarized in Table 1.

3. Characterization

3.1. XRD pattern

To identify the crystallite phase of the as-synthesized CdS and Cu_2O semiconductors and their corresponding composite, their XRD patterns were recorded and are shown in Figs. 1a–d. All important peaks are assigned by corresponding *hkl* plans. Generally, CdS crystals have two important crystallite phases of the hexagonal wurtzite and cubic zinc blend [30,31]. Its hexagonal (wurtzite) phase crystals have six main diffraction peaks of (100), (002), (101), (110), (103) and (112) correspond to 2θ values of 24.96°,

Table 1
Change in initial pH of SFSZ solutions during the study of some pivotal parameters in its photodegradation by the Cu_2O-CdS composite

Parameter	Value	Initial pH	Final pH
Blank	–	4.8	4.8
Direct photolysis	–	4.8	7.7
CdS/Cu_2O	1:1	4.8	8.0
	1:2	6.0	8.3
	1:3	6.0	8.0
	1:4	6.3	8.0
	2:1	6.6	8.0
	3:1	6.3	7.7
	4:1	6.5	8.0
C_{SSZ} (mg L^{-1})	10	6.0	7.2
	20	6.3	7.3
	30	5.8	7.5
	40	7.0	7.9
	50	7.3	7.3
Catalyst dose (g L^{-1})	0.1	5.8	7.8
	0.3	6.0	8.3
	0.5	6.3	8.0
	1.0	6.7	8.5

26.63°, 28.31°, 43.71°, 47.86° and 51.85°, respectively (JCPDS No. 41-1049), accompanied with two weaker peaks of (203) and (210) at 2θ values of 66.61° and 69.09°, respectively [32]. In contrast, the cubic (zinc blend, β-CdS) phase CdS crystals have main peaks at 2θ values of 26.7°, 44° and 52° correspond to scattering from the (111), (220) and (311) planes (JCPDS 00-042-1411) [33]. As shown in Fig. 1a, the XRD pattern of as-synthesized CdS agree with that of cubic CdS phase. Broadening of the peaks confirms formation of small particles during the synthesis process. Fig. 1b shows typical XRD pattern of the as synthesized Cu_2O crystals. Corresponding peaks of Cu_2O at 2θ values of 29.58° (110), 36.5° (111), 42.36° (200), 61.64° (220), 73.62° (311) and 77.62° (222) are inconsistent with its cubic phase based on JCPDS# 65-3288 [34,35]. As shown in Fig. 1c, corresponding peaks of both CdS and Cu_2O crystals are present in the XRD pattern of the CdS-Cu_2O composite. All patterns were comprised in Fig. 1d. This comparison shows broader peaks for CdS crystals, confirming smaller particle size and lower crystallinity for CdS NPs. In contrast, the intense peaks of Cu_2O confirms a higher crystallinity for Cu_2O crystals. In addition, decrease in peak intensity of the composite is due to decrease in Cu_2O component with respect to its pure crystals.

By using the Scherrer equation and peaks' width, the crystallite size (d) of the composite was estimated that varied from 6 to 38 nm according different peaks' width of the investigated XRD peaks. In the following Scherrer equation,

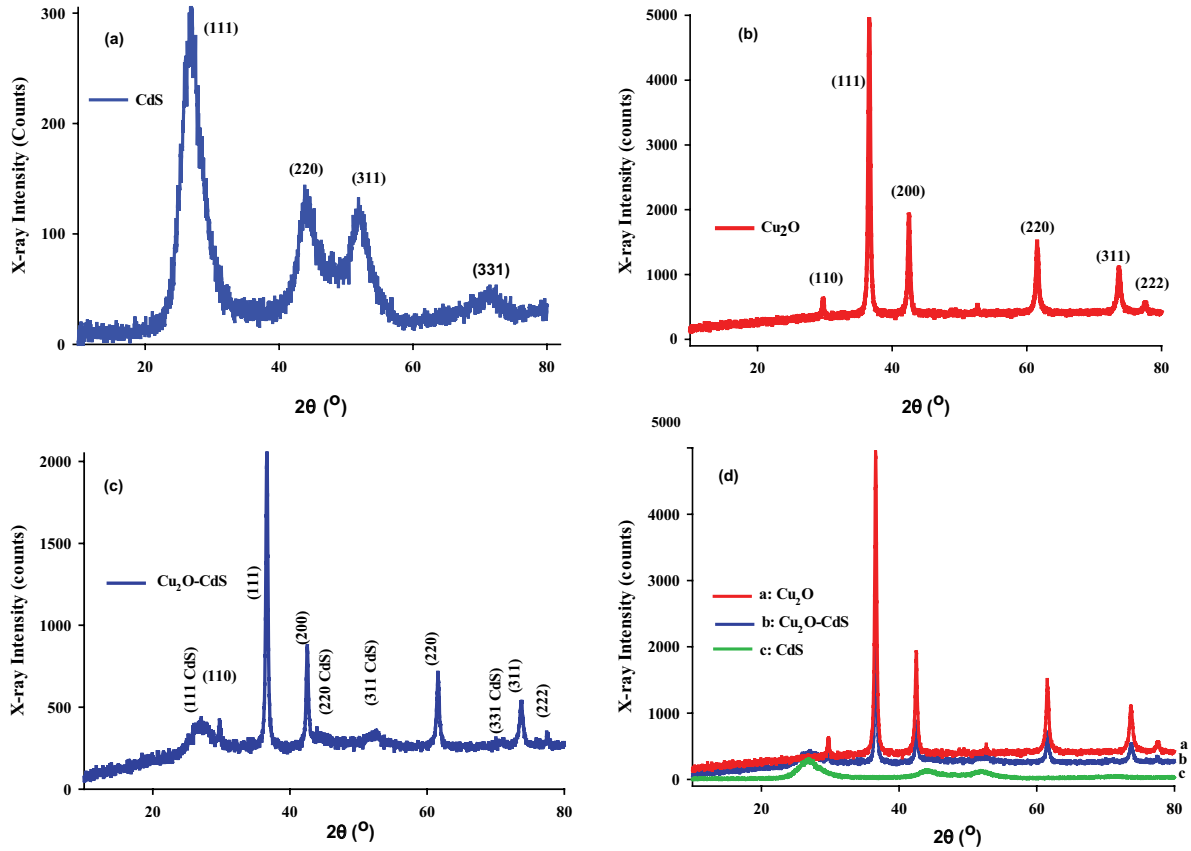

Fig. 1. Typical XRD pattern recorded for the as-synthesized CdS and Cu_2O semiconductors and the CdS-Cu_2O composite (CdS/Cu_2O mole ratio of 1:2).

λ shows the applied X-ray wavelength (1.5406 Å), θ the Bragg angle, K the Scherrer constant (0.9) and β shows the full width at half maximum [36].

$$d = \frac{K\lambda}{\beta \cos\theta} \quad (2)$$

3.2. Optical properties and scanning electron microscope images

To follow the change in band gap energies of the used semiconductors after coupling process, UV–Vis diffuse reflectance spectroscopy (UV–Vis DRS) was used and the resulted reflectance spectra are shown in Fig. 2a. The best method for the estimation of band gap energies is the Kubelka–Munk model and Tauc plots [37–40]. A typical Tauc plot for the allowed direct electronic transition is shown in Fig. 2b. The band gap values of 2.27, 2.30 and 2.39 eV were estimated for this electronic transition of CdS, Cu_2O and their composite, respectively. These values show a relative blue shift for the synthesized nanoparticles with respect to the bulk CdS and Cu_2O semiconductors. A blue shift was also observed in band gap energy of the composite with respect to the single systems. Similar blue shift has observed for CdS-SnO_2 composite that was prepared by impregnation method. The blue shift in band gap energy of the composite with respect to the mono-component semiconductors has related to Cd-O-Sn linkages at the interface of the composite sample [41,42].

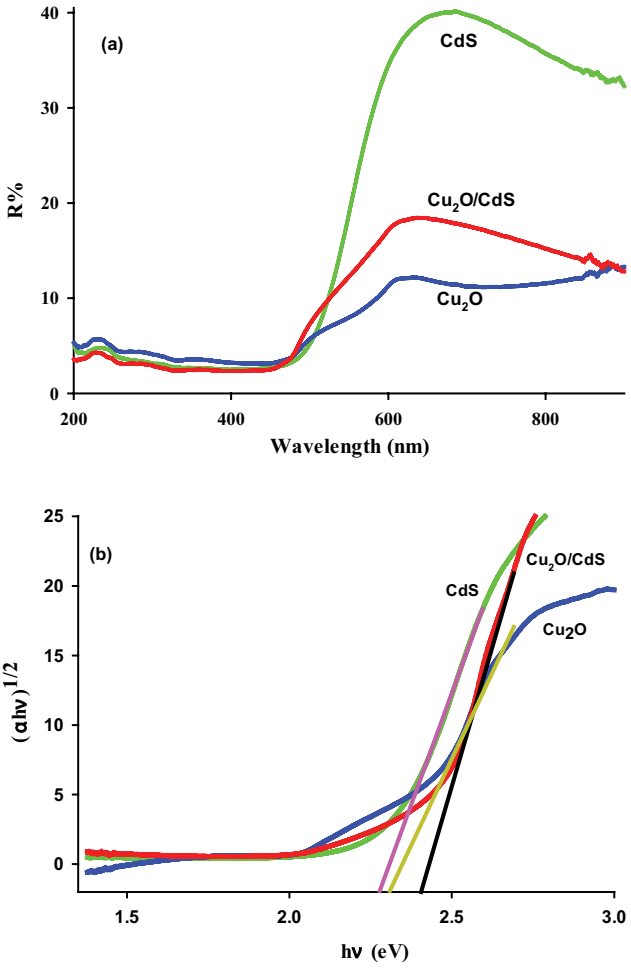

Fig. 2. (a) UV–Vis reflectance spectra for the single and composite (with CdS/Cu_2O mole ratio of 1:2) samples and (b) corresponding Tauc plots for allowed direct electronic transition for the samples.

Fig. 3 shows some FESEM images of the as-synthesized Cu_2O-CdS composite, confirming that the composite has nano-dimension. All SEM images showed cubic crystals for the composite. Some crystals have ordered cubic shape that can be related to Cu_2O crystals as discussed in XRD section, because it showed intense and narrow XRD peaks. In contrast, CdS crystals with broad XRD peaks should show lower crystallinity, and hence the cubic phase with lower ordered shape can be related to CdS crystals. The CdS crystals partially aggregated, while the Cu_2O ones present as single cubic crystals. The CdS crystals were relatively well dispersed through the composite and due to the higher mole ratio of Cu_2O (2:1), it consisted major parts of the composite.

Fig. 4 shows some selected TEM images of the Cu_2O-CdS composite. As shown, nano-dimension of the composite can be confirmed from the images. Also, the ordered cubic phase of Cu_2O crystals accompanied with CdS cubic crystals with lower ordered shape were appeared in TEM images. These pictures give similar information that obtained and discussed by scanning electron microscope (SEM) images.

3.3. Photodegradation studies

3.3.1. Boosting effect of coupling of Cu_2O and CdS and effect of their mole ratio

Based on preliminary experiments, effect of surface adsorption by the as-synthesized Cu_2O-CdS composite in removal of SFSZ was investigated and the results showed that about 7% of SFSZ molecules can be removed by the composite at dark condition during 25 min. No significant change was obtained for this removal method after 4–5 min and hence before the photodegradation experiments, the suspensions were shaken at dark for 5 min to adsorption/desorption process reached to equilibrium (Fig. 5a). As shown, direct photolysis can remove about 13.8% of SFSZ molecules during 25 min. This confirms visible light alone cannot create reactive radicals for destroying SFSZ molecules.

As shown after using the photocatalysis process by single semiconductors, the removal efficiency of SFSZ was remarkably enhanced because both Cu_2O and CdS semiconductors can excite by the arrived visible photons for the production of reactive e/h pairs and OH and superoxide radicals. But, when the Cu_2O-CdS composite was used, the degradation efficiency was strikingly increased, confirming the positive role of combination of these semiconductors to enhance charge carriers' transfer. This is due to well-matched standard potentials between C_b levels of the coupled system as well as the values for their V_b levels. Although in some particles both Cu_2O and CdS semiconductors can produce e/h pairs, they may recombine and act as single semiconductors. But, in some particles, the photogenerated electrons in Cu_2O-C_b level immigrate to that of CdS because of its more negative potential. This internal reduction–oxidation

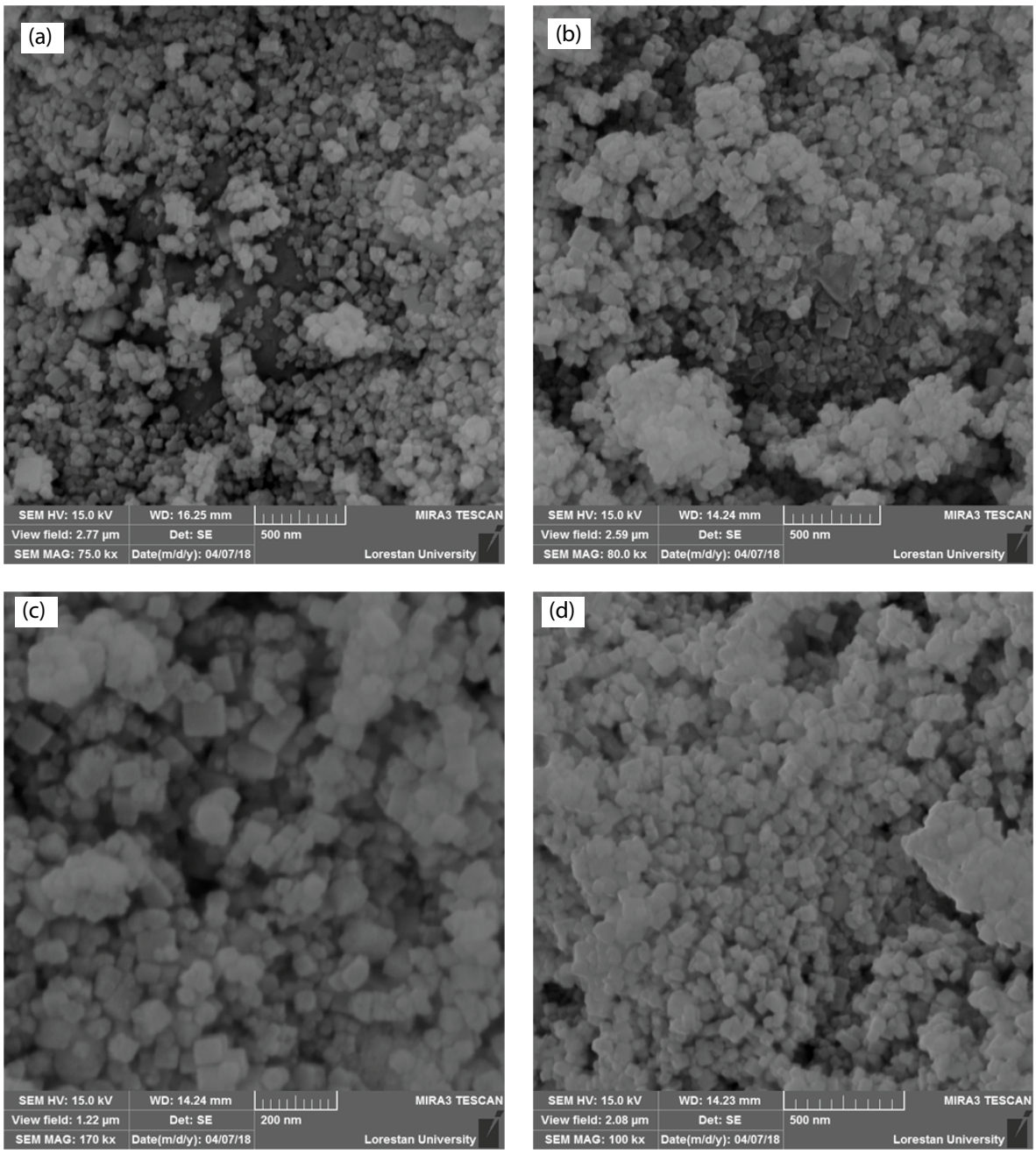

Fig. 3. Some selected FESEM images for the as-synthesized Cu_2O-CdS NPs (with CdS/Cu_2O mole ratio of 1:2).

process elongates lifetime of the photogenerated e/h pairs and enhances the degradation efficiency (Fig. 5c).

Change of mole ratio of CdS/Cu_2O changed the photodegradation ability of the resulted composites as shown in Fig. 5b. As shown, when moles of Cu_2O is twice the CdS the best activity was obtained for the composite. This confirms that in this ratio, the best conditions are provided for electron transfer from Cu_2O-C_b to CdS-C_b. When moles of Cu_2O is about 3–4 times greater than CdS, the photocatalytic activity was drastically decreased and when moles of CdS tend to increase to three times greater than Cu_2O, the activity was relatively increased. The results confirm that in addition of matched potentials in a coupled semiconducting system, their mole ratio also plays a vital role in charge carriers' separation [43,44].

3.3.2. Kinetic aspect of the process

In a heterogeneous photodegradation process, adsorption of both of the oxidant and the pollutant is a pivotal parameter in kinetic point of view. When this process is an equilibrium process, its kinetics can be interpreted by the Langmuir–Hinshelwood (L-H) model. This model supposes that both species present in a monolayer at the

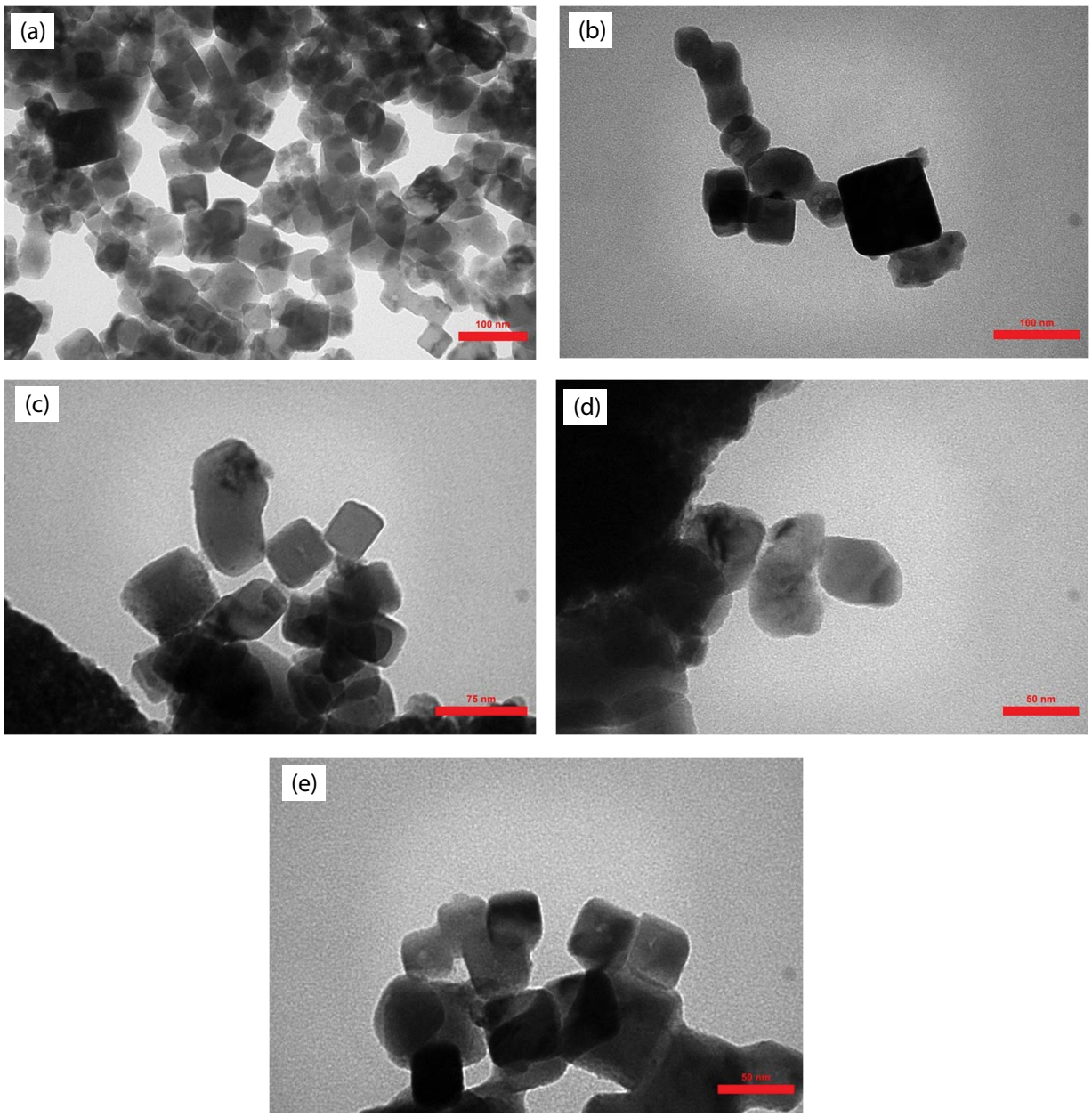

Fig. 4. Some TEM images for the as-synthesized Cu_2O-CdS NPs.

solid–liquid interface and control the rate-determining step of the process. In the following L-H equation, the reaction rate (r in mg/L min) relates to the specific reaction rate constant (k' in mg/L min) and the equilibrium constant of the reactant (K in L/mg) and the concentration of the pollutant (C).

$$r = -\frac{dC}{dt} = \frac{k'\,KC}{1+KC} = k'\,\theta \tag{3}$$

By integrating Eq. (3), logarithmic form of the equation can be yield (Eq. (4)) which is similar to an apparent first-order equation. In the final equation, C_0 and C_t stand for the initial and final concentrations of the pollutant, respectively, t is irradiation time and k shows apparent first-order rate constant [45–47]. Eq. (3) is a zero order at high concentrations ($C > 5 \times 10^{-3}$ mol L^{-1}) but at concentrations below 1×10^{-3} mol L^{-1} the reaction obeys from an apparent first-order reaction.

$$\ln\left(\frac{C_0}{C}\right) + k'\left(C_0 - C_t\right) = k'\,Kt = kt \tag{4}$$

For study of the kinetics of the process as a function of concentration of SFSZ, photodegradation experiments were done at different concentrations of SFSZ. Decrease in UV–Vis absorbance of a 20 mg L^{-1} of SFSZ solution, as an example, is shown in Fig. 6a, which shows decrease in the absorbance intensity during time that accompanied an about 30 nm red

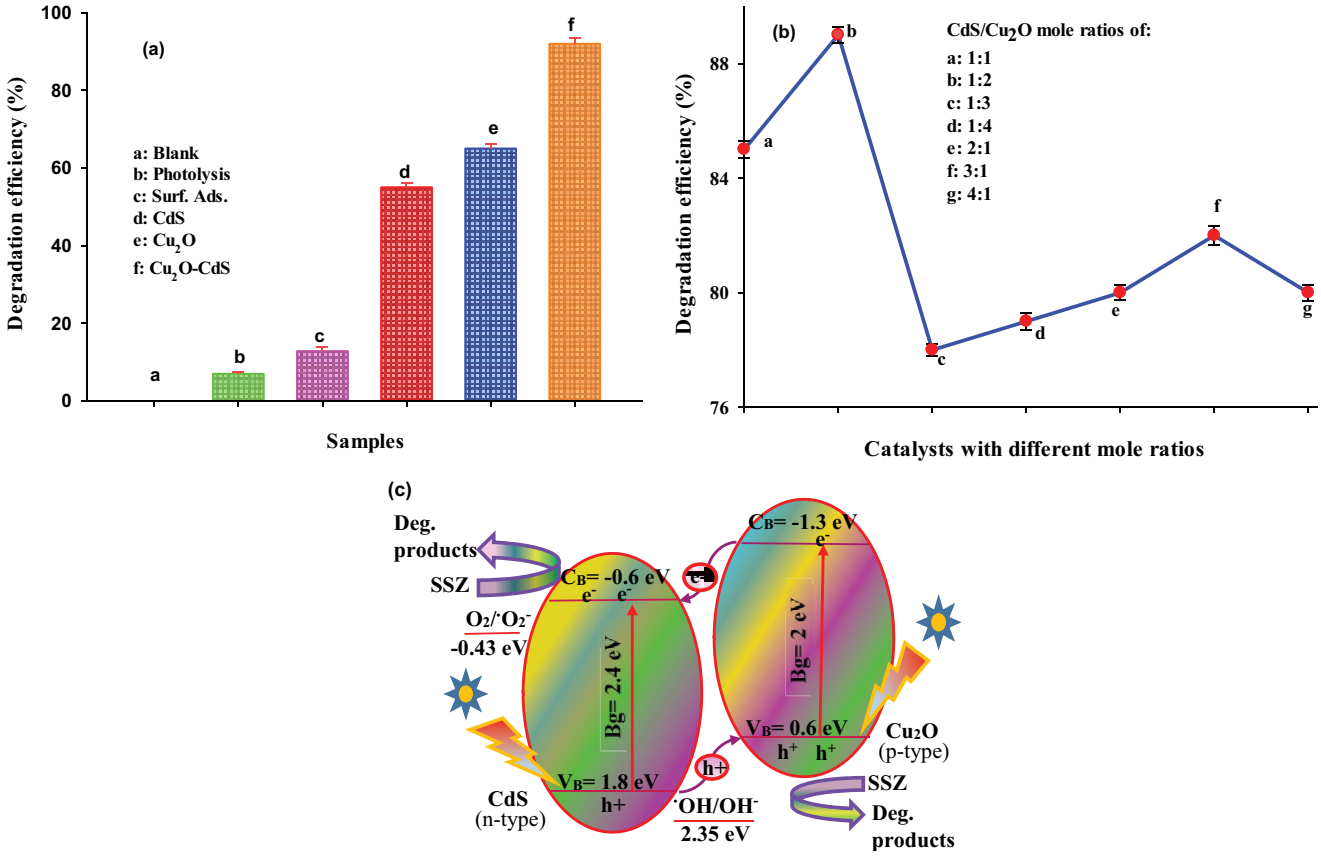

Fig. 5. Effects of surface adsorption, direct photolysis and photocatalytic processes on SFSZ removal (catalysts dose 0.3 g L^{-1}, C_{SFSZ}: 10 mg L^{-1}, irradiation time: 25 min, initial pH: 4.6), (b) effects of the mole ratio of the CdS/Cu_2O in photodegradation of SFSZ at the conditions in part A; All results were averaged based on triplicates measurements, and (c) the energy diagram for the charge carriers' transfer in the Cu_2O-CdS composite.

shift in maximum absorption peak. Corresponding relative decrease in concentration of SFSZ during the photodegradation process for different concentration is shown in Fig. 6b. Although a 10 mg L^{-1} SFSZ solution showed the lowest C/C_0 value but the moles of the degraded SFSZ molecules is very low. In general, the degradation percentages of 92%, 82%, 78%, 76% and 36% were, respectively, obtained for 10, 20, 30, 40 and 50 mg L^{-1} of SFSZ solutions at the end of photodegradation process. These values show 230, 410, 585, 760 and 450 nano-moles of SFSZ molecules were degraded during about 15 min of photodegradation process, confirming a fast photodegradation process. These confirm the best degradation extent for 30 and 40 mg L^{-1} SFSZ solutions. Typical plots of Hinshelwood equation are shown in Fig. 6c. From the slopes of the curves, the apparent rate constants were estimated and summarized in Table 2. As shown, the best rate constant and the fastest rate was obtained for a 30 mg L^{-1} of SFSZ solution.

In general, collision probability between SFSZ molecules and the produced reactive radicals at the surface of the catalyst (or with catalyst surface, in general) has a prime importance in photodegradation efficiency because of the short lifetime of the produced OH and superoxide radicals (about nano-second) and e/h pairs [48]. This important was achieved at 30 and 40 mg L^{-1} of SFSZ solutions (especially for 30 mg L^{-1} because of its higher rate constant). At higher concentrations, a major part of the arrived photons may be screened by high SFSZ molecules that are present in media [49].

Change in initial pH of SFSZ solutions during the photodegradation process was also followed for different concentrations and the results are shown in Fig. 6d. As shown, as the photodegradation process proceeded initial pH of the suspensions was increased and reached neutral and even to relatively low alkaline pHs (near 8). Molecular structure of SFSZ is shown in Fig. 6e. The results confirms that all acidic functional groups (such as carboxylic acid in salicylic ring of the structure) or other organic acids formed during the photodegradation process were successfully mineralized. This also confirms some amines may be formed during the breaking of nitrogen contained bonds that can be hydrolyzed to increase the solution pH. As shown, the maximum change in pH was observed for 30 mg L^{-1} of SFSZ solution that showed the maximum rate constant.

The results belong to the kinetic aspect of the process as the function of dosage of CdS/Cu_2O catalyst are shown in Fig. 7a and Table 2. As shown in Table 2, the best and faster rate was observed when a 0.5 g L^{-1} of the catalyst was used. In general, sufficient amount of the catalyst should be present in the media for providing sufficient active sites for the catalytic process without disruption of clarity of the suspensions.

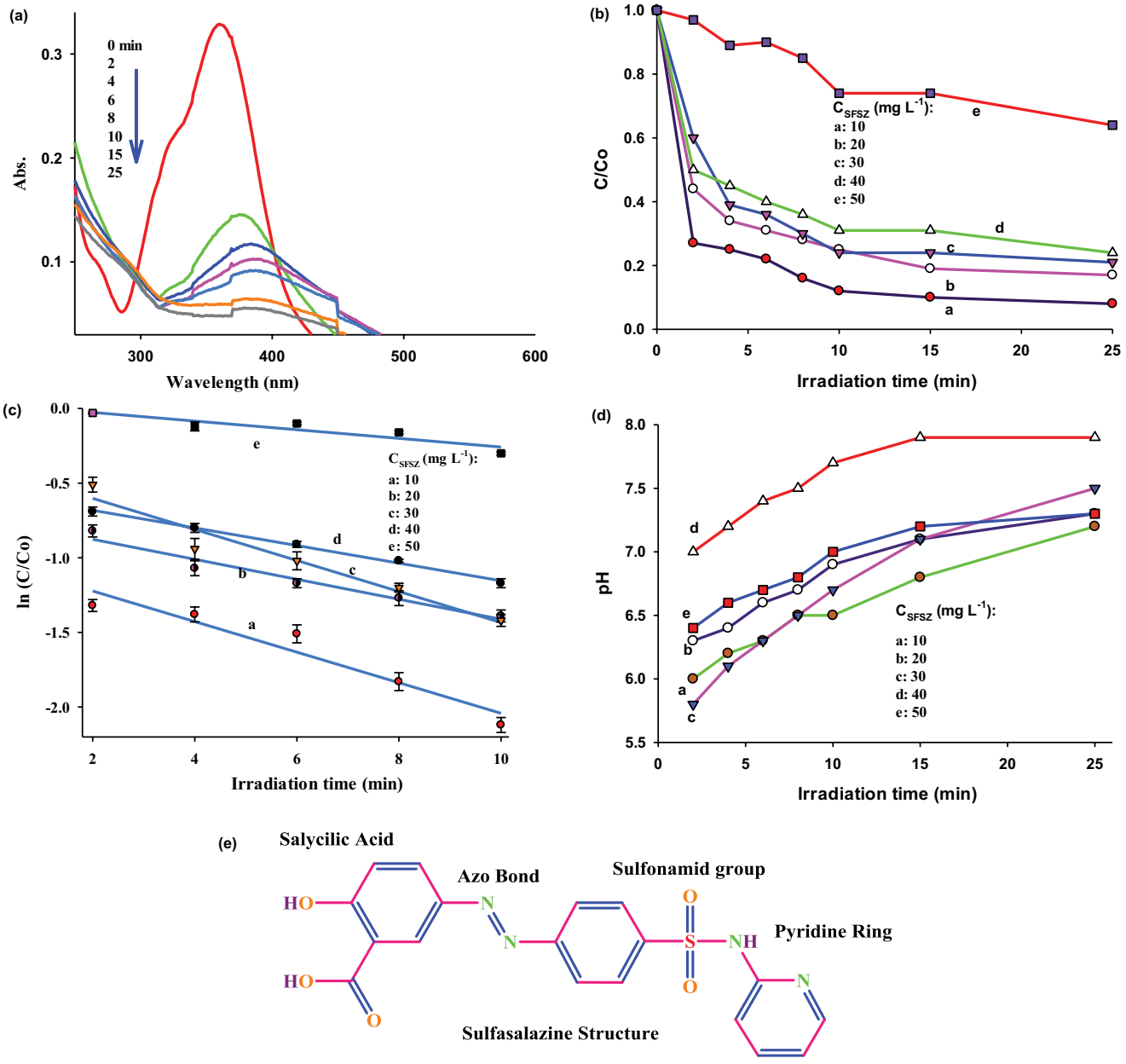

Fig. 6. (a) Change in UV–Vis absorption spectra of a 20 mg L^{-1} of SFSZ solution during the photodegradation process, (b) Change in C/C_0 values during the irradiation process in photocatalytic degradation of SFSZ by Cu_2O-CdS catalyst, (c) resulted ln (C/C_0) – time plots constructed for study of the kinetics of the process as a function of SFSZ concentration in time interval of 2–10 min (conditions: catalysts dose 0.5 g L^{-1}, irradiation time: 25 min, initial pH: 4.9–6.5), and (d) change in initial pH of SFSZ solution during its photodegradation process for different concentrations of SFSZ.

On the other hand, high amounts of the catalyst strikingly scatter the arrived photons and hence photoexcitation of the catalyst significantly decreased. Here, the best conditions for achieving the best degradation rate are provided at 0.5 g L^{-1} of the catalyst.

Fig. 7b shows the results belong to the effect of solution pH on the kinetic aspect of the process. Higher rate constant value was obtained for pH 5 as shown in Table 2. The pH_{PZC} (point of zero charge pH) of the catalyst was estimated about 6.9 according to the procedure described in literature [50]. The sulfonamide hydrogen has a pKa value of 6.8 and nitrogen atoms in azo bond or pyridine ring have a pKa value of 11. At pH 3 these functional groups are present in the protonated form. This results a repulsive force with the positive charges of the catalyst surface at pHs below pH_{PZC}. The carboxylic acid functional group in the salicylic ring has a pKa value of 2.4. Hence at pHs above pH_{PZC} this functional group together with sulfonamide functional group are present as deprotonated form, resulting in a repulsive force between these anionic form or the free electron pairs of

Table 2
Hinshelwood equation and apparent first-order rate constants obtained

Parameter	Value	$K \times 10^{-2}$ (min^{-1}) ± SD (n = 3)	Equation	R^2
	10	**9.30 ± 0.90**	$Y = -0.093x - 0.991$	0.9103
	20	6.70 ± 0.50	$Y = -0.067x - 0.692$	0.9503
C_{SFSZ} (mg L^{-1})	**30**	**11.7 ± 1.30**	$Y = -0.117x - 0.256$	0.9318
	40	5.90 ± 0.30	$Y = -0.059x - 0.538$	0.9925
	50	2.80 ± 0.05	$Y = -0.028x - 0.430$	0.8625
	0.3	8.50 ± 0.40	$Y = -0.085x + 0.117$	0.9371
Catal. Dos. (g L^{-1})	**0.5**	**8.90 ± 0.20**	$Y = -0.089x - 0.538$	0.9351
	1.0	7.60 ± 0.20	$Y = -0.076x - 0.216$	0.9284
	3	5.00 ± 0.10	$Y = -0.050x - 0.091$	0.9546
pH	**5**	**9.10 ± 0.20**	$Y = -0.91x - 0.533$	0.9554
	7	6.60 ± 0.30	$Y = -0.066x - 0.323$	0.9110

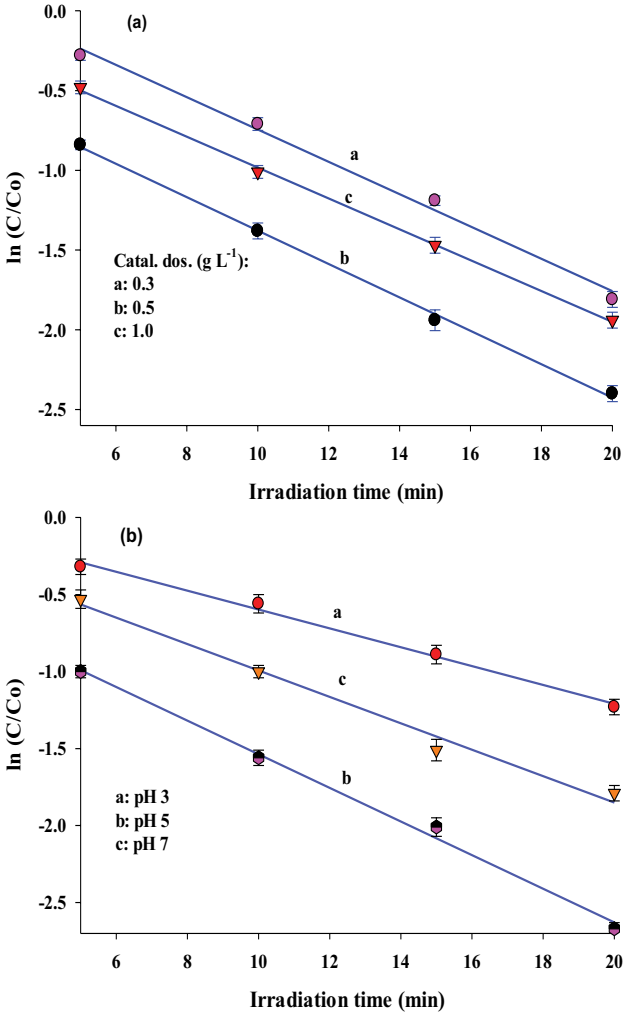

Fig. 7. (a) Plots for study of the kinetic of the process as a function of dosage of the CdS-Cu_2O catalyst (conditions: C_{SFSZ}: 10 mg L^{-1}, irradiation time: 25 min, initial pH: 4.5–6.7) and (b) typical ln (C/C_0) – time plots constructed for study of the kinetic of the process as a function of initial pH of SFSZ solution (conditions: catalysts dose 0.5 g L^{-1}, C_{SFSZ}: 10 mg L^{-1}, irradiation time: 25 min).

nitrogen atoms with negatively charged catalyst surface. Best interactions between SFSZ molecules and the catalyst surface are present at pH around pH_{PZC}. Here, the best photodegradation rate was obtained at pH about 5, because at this pH the surface of the catalyst is relatively protonated while some aforementioned nitrogen atoms are present in deprotonated form, resulting an attractive force to bring SFSZ molecules near the catalyst surface [40,51].

3.3.3. COD and high-performance liquid chromatography studies

Chemical oxygen demand (COD) gives a measure of the required oxygen for destroying the organic matters present in solution and hence its value counts as a measure of the pollution extent of water samples. Accordingly, high COD value means high pollution of the investigated water sample [52]. In this regard, the SFSZ solutions were subjected to the common COD method [53] for estimation of the photodegradation extent of SFSZ molecules. As shown in Table 3, about 72% of SFSZ molecules were mineralized during initial 15 min of the process, confirming a relatively fast photodegradation process.

The high-performance liquid chromatograms (HPLC) of SFSZ solutions before and after 25 min photodegradation process are shown in Fig. 8a. As shown, peak area of the sample at retention time of 16.05 min was drastically decreased during the photodegradation process, confirming

Table 3
Results of COD studies during photodegradation of SFSZ by the optimized catalysts at the optimized conditions

Irrad. time (min)	COD (mg O_2/L)		Deg. efficiency (%)
	Initial	Final	
0	1,248	1,248	–
15	1,248	320	72
25	1,248	224	82
35	1,248	192	84

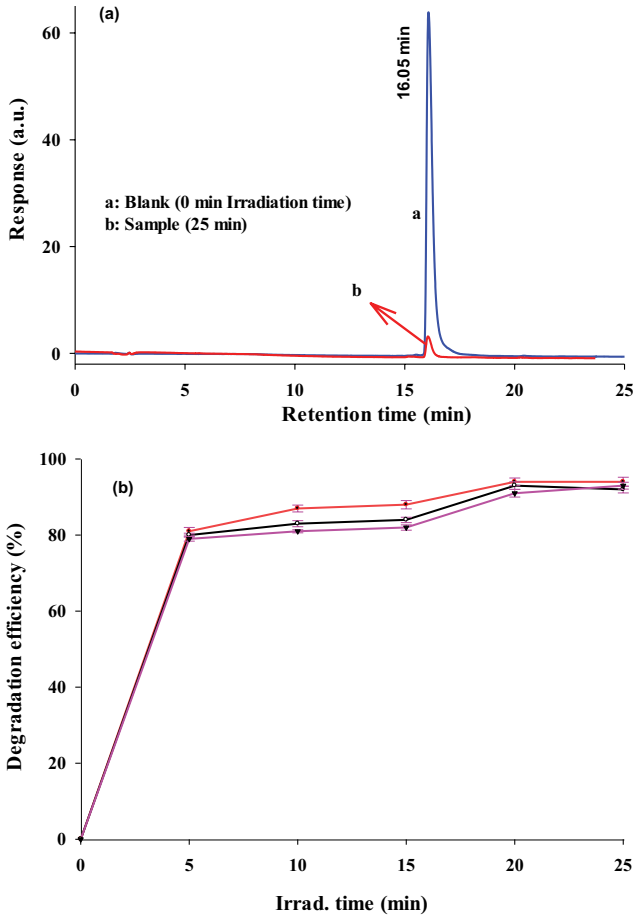

Fig. 8. (a) Typical HPLC obtained for SFSZ solution before and after photodegradation process (conditions for photodegradation experiment: catalyst dose: 0.5 g L^{-1}, C_{SFSZ}: 10 mg L^{-1}, irradiation time: 25 min, initial pH: 5) and (b) reusing results obtained in successive using of the catalyst in SFSZ photodegradation in the aforementioned conditions.

the degradation of SFSZ molecules into the smaller fragments. Using the peak area of the peaks, degradation extent of 94.7% was estimated for the degradation of SFSZ molecules during 25 min photodegradation process. Presence of no additional peaks confirms that mineralization of SFSZ molecules is relatively high. This may confirm that some degradation intermediates cannot be detected by detector of the instrument.

Comparison of the results confirms that 94%, 94.7% and 82% of SFSZ molecules were degraded as detected by UV–Vis spectroscopy, high-performance liquid chromatography and COD results during 25 min photodegradation process. As shown, the results estimated by UV–Vis spectroscopy and high-performance liquid chromatography are very close. The used wavelength in UV-detector of high-performance liquid chromatography is 345 nm and in UV–Vis spectroscopic measurements λ_{max} is 360 nm. This confirms that in both methods similar molecules were detected by detectors that is original SFSZ molecules that not degraded. As shown, COD results show lower degradation extent, confirming appearance of some intermediates that persist to further degradation during shorter photodegradation periods. These relatively resistant intermediates may be degraded during longer photodegradation times.

3.3.4. Reusing results

Due to economic importance of any suggested method/catalyst, etc., the as-synthesized composite was used in successive runs in the degradation of SFSZ at the following conditions: catalyst dose: 0.5 g L^{-1}, C_{SFSZ}: 10 mg L^{-1}, irradiation time: 25 min, initial pH: 5. The obtained results are shown in Fig. 8b. Each experiment at each time was repeated three times. As shown, the suggested composite retained its catalytic activity during three successive runs and no considerable decrease in its photocatalytic activity was observed.

3.3.5. Scavenger study

The scavengers effects of NaCl, Na_2CO_3, Na_2SO_4 and ascorbic acid (AA) on the photocatalytic activity of the Cu_2O–CdS composite was studied which of results during 30 min irradiation process are summarized Table 4. Carbonate, sulfate and AA are well-known scavengers for $^{\bullet}OH$ radicals, the photogenerated electrons and superoxide radicals, respectively. Chloride anions plays a dual role scavenging effect and can scavenge both the photogenerated holes and hydroxyl radicals simultaneously. This study tell us the importance of each reactive component in the degradation of SFSZ molecules. In general, presence of each scavenging agent used in this study decreased the photodegradation extent of SFSZ molecules by the composite. Also, increasing in the concentration of each scavenger caused to higher decrease in the activity of the catalyst. These observations confirm that all reactive species including the photogenerated e/h pairs, hydroxyl and super-oxide radicals have participated in SFSZ degradation.

After scavenging process, some novel radicals such as ascorbyl radical ($AH^{\bullet}$), $Cl_2^{\bullet-}$, $Cl^{\bullet}$, $HClO^{-\bullet}$, $ClO^{\bullet}$, $SO_4^{\bullet-}$, etc. may be formed corresponding to the used scavenging agent. Decreased efficiency of the catalyst in the presence of the used scavenging agents confirms that the produced novel radicals have lower oxidation power than the OH or superoxide radical. In addition, it has reported that such inorganic salts have smaller sizes and hence they can rapidly occupy the active sites on the surface of the catalyst. Hence, lower SFSZ molecules can be adsorbed on the catalyst surface. Also, these adsorbed inorganic ions react with the photogenerated e/h pairs, OH and superoxide radicals. Hence, photodegradation efficiency was decreased in the presence of such anions [54–60].

Based on the results in Table 4, the following scavenging trend was observed.

$$Cl^- > SO_4^{2-} > CO_3^{2-} > \text{Ascorbic Acid}$$

As mention above, chloride anions have a dual role and can scavenge both the OH radicals and holes. Comparison of the effects of chloride and bicarbonate anions confirms that effect of the photogenerated holes is much significant with respect to the OH radicals in SFSZ degradation. Generally, the aforementioned trend confirms the photogenerated e/h

Table 4
Effect of different scavenging agents on the photodegradation extent of SFSZ molecules by the Cu_2O–CdS composite (catalyst dose: 0.5 g L^{-1}, C_{SFSZ}: 10 mg L^{-1}, irradiation time: 30 min, initial pH: 5)

Scavenger Role	Scavengers	C (mM)	Degradation% ± SD (n = 3)
–	–	–	**80 ± 0.0050**
		10	34 ± 0.0040
Hole Scavenger	Cl^-	30	36 ± 0.0030
		50	**28 ± 0.0020**
		10	74 ± 0.0028
•OH Scavenger	CO_3^{2-}	30	67 ± 0.0026
		50	**43 ± 0.0057**
		10	52 ± 0.0010
Electron Scavenger	SO_4^{2-}	30	45 ± 0.0020
		50	**37 ± 0.0010**
		10	61 ± 0.0050
$O_2^{\bullet-}$ Scavenger	Asc. acid	30	60 ± 0.0026
		50	**55 ± 0.0026**

pairs have better role than OH and super-oxide radicals in SFSZ photodegradation.

When we comprise standard potentials of valence and conduction bands of the involved semiconductors in the composite (See Z-scheme in Fig. 5c), it can be concluded that superoxide radicals can be produced by the photogenerated electrons in Cu_2O-C_b (E^0: –1.3 V, E^0 $O_2/^{\bullet}O_2$: –0.43 V). In addition, both the photogenerated holes in the V_b-Cu_2O and V_b-CdS levels have suitable potentials to oxidize water molecules or hydroxyl anions to form hydroxyl radicals ($E^0_{V_b}$: Cu_2O = 0.6 V; CdS = 1.8 V, $^{\bullet}OH/^{-}OH$: 2.38 V). The oxidation potential of 0.75 V vs. Ag/AgCl reference electrode (0.98 V vs. SHE) has reported for the oxidation of SFSZ molecules [61]. These values confirm that both aforementioned holes can easily oxidize SFSZ molecules. Its oxidation by superoxide radicals is relatively hard with respect to its oxidation by the holes. Although, all the aforementioned reactive species have suitable role in SFSZ degradation, but the photogenerated holes showed a better role.

4. Conclusion

The boosted activity of the Cu_2O-CdS composite with respect to single Cu_2O and CdS semiconductors confirms that the matched potentials of C_b and V_b levels and mole ratio in a coupled semiconducting system play the vital roles in charge carriers' separation and photodegradation activity. Obeying of the kinetic of the process from Langmuir–Hinshelwood model confirms mono-layer adsorption of the pollutant onto the catalyst surface. The degradation extents of 92%, 82%, 78%, 76% and 36% were, respectively, obtained for 10, 20, 30, 40 and 50 mg L^{-1} of SFSZ solutions at the end of photodegradation process. Although, lower concentrations showed higher degradation percentages, but when these values converted to the degraded moles of SFSZ, the results showed 230, 410, 585, 760 and 450 nano-moles of SFSZ molecules were degraded during about 15 min, confirming a fast photodegradation process. Also, a 30 mg L^{-1} of SFSZ solution showed the maximum apparent rate constant confirming maximum collision probability is present for SFSZ molecules and OH/superoxide radicals or catalyst surface in this concentration. Effects of some scavenging agents showed better role of the photogenerated holes in the degradation of SFSZ molecules.

References

[1] P. Bansal, A. Verma, N, Ag co-doped TiO_2 mediated modified in-situ dual process (modified photocatalysis and photo-Fenton) in fixed-mode for the degradation of Cephalexin under solar irradiations, Chemosphere, 212 (2018) 611–619.

[2] A. Heidarineko, A. Bagheri Ghomi, P-type semiconducting NiO nanoparticles synthesis and its photocatalytic activity, Iran. J. Catal., 7 (2017) 277–282.

[3] P. Raizada, J. Kumari, P. Shandilya, P. Singh, Kinetics of photocatalytic mineralization of oxytetracycline and ampicillin using activated carbon supported ZnO/$ZnWO_4$ nanocomposite in simulated wastewater, Desal. Wat. Treat., 79 (2017) 204–213.

[4] Z. Amani-Beni, A. Nezamzadeh-Ejhieh, NiO nanoparticles modified carbon paste electrode as a novel sulfasalazine sensor, Anal. Chim. Acta, 1031 (2018) 47–59.

[5] Y. Ji, Y. Yang, L. Zhou, L. Wang, J. Lu, C. Ferronato, J.M. Chovelon, Photodegradation of sulfasalazine and its human metabolites in water by UV and UV/peroxydisulfate processes, Water Res., 133 (2018) 299–309.

[6] J.-J. Li, S.-C. Cai, Z. Xu, X. Chen, J. Chen, H.-P. Jia, J. Chen, Solvothermal syntheses of Bi and Zn co-doped TiO_2 with enhanced electron-hole separation and efficient photodegradation of gaseous toluene under visible-light, J. Hazard. Mater., 325 (2017) 261–270.

[7] Z. Ye, J. Li, M. Zhou, H. Wang, Y. Ma, P. Huo, L. Yu, Y. Yan, Well-dispersed nebula-like ZnO/CeO_2@HNTs heterostructure for efficient photocatalytic degradation of tetracycline, Chem. Eng. J., 304 (2016) 917–933.

[8] X. Wang, J. Jia, Y. Wang, Combination of photocatalysis with hydrodynamic cavitation for degradation of tetracycline, Chem. Eng. J., 315 (2017) 274–282.

[9] N. Masoudipour, M. Sadeghi, F. Mohammadi-Moghadam, Photo-catalytic inactivation of E. coli using stabilized Ag/S, N-TiO_2 nanoparticles by fixed bed photo-reactor under visible light and sunlight, Desal. Wat. Treat., 110 (2018) 109–116.

[10] A. Buthiyappan, A.R. Abdul Aziz, W.M.A.W. Daud, Recent advances and prospects of catalytic advanced oxidation process in treating textile effluents, Rev. Chem. Eng., 32 (2015) 1–47.

[11] V.K. Gupta, A. Fakhri, M. Azad, S. Agarwal, Synthesis and characterization of Ag doped ZnS quantum dots for enhanced photocatalysis of Strychnine as a poison: charge transfer behavior study by electrochemical impedance and time-resolved photoluminescence spectroscopy, J. Colloid Interface Sci., 510 (2018) 95–102.

[12] P. Dhiman, M. Naushad, K.M. Batoo, A. Kumar, G. Sharma, A.A. Ghfar, G. Kumar, M. Singh, $FexZn_{1-x}O$ as a tuneable and efficient photocatalyst for solar powered degradation of bisphenol A from aqueous environment, J. Cleaner Prod., 165 (2017) 1542–1556.

[13] B.A. Ünnü, G. Gündüz, M. Dükkancı, Heterogeneous Fenton-like oxidation of crystal violet using an iron loaded ZSM-5 zeolite, Desal. Wat. Treat., 57 (2016) 11835–11849.

[14] A. Eslami, A. Oghazyan, M. Sarafraz, Magnetically separable $MgFe_2O_4$ nanoparticle for efficient catalytic ozonation of organic pollutants, Iran. J. Catal., 8 (2018) 95–102.

[15] Z. Wang, H. Zhang, H. Cao, L. Wang, Z. Wan, Y. Hao, X. Wang, Facile preparation of ZnS/CdS core/shell nanotubes and their enhanced photocatalytic performance, Int. J. Hydrogen Energy, 42 (2017) 17394–17402.

[16] Y. Ma, X. Li, Z. Yang, S. Xu, W. Zhang, Y. Su, N. Hu, W. Lu, J. Feng, Y. Zhang, Morphology control and photocatalysis

enhancement by in situ hybridization of cuprous oxide with nitrogen-doped carbon quantum dots, Langmuir, 32 (2016) 9418–9427.
[17] N.L. Subbulekshmi, E. Subramanian, Nano CuO immobilized fly ash zeolite Fenton-like catalyst for oxidative degradation of p-nitrophenol and p-nitroaniline, J. Environ. Chem. Eng., 5 (2017) 1360–1371.
[18] H.R. Pouretedal, M. Fallahgar, F.S. Pourhasan, M. Nasiri, Taguchi optimization of photodegradation of yellow water of trinitrotoluene production catalyzed by nanoparticles TiO_2/N under visible light, Iran. J. Catal., 7 (2017) 317–326.
[19] S. Zinatloo-Ajabshir, M. Salavati-Niasari, Facile synthesis of nanocrystalline neodymium zirconate for highly efficient photodegradation of organic dyes, J. Mol. Liq., 243 (2017) 219–226.
[20] N. Sapawe, A.A. Jalil, S. Triwahyono, One-pot electrosynthesis of ZrO_2–ZnO/HY nanocomposite for photocatalytic decolorization of various dye-contaminants, Chem. Eng. J., 225 (2013) 254–265.
[21] S. Landi Jr, J. Carneiro, S. Ferdov, A.M. Fonseca, I.C. Neves, M. Ferreira, P. Parpot, O.S.G.P. Soares, M.F.R. Pereira, Photocatalytic degradation of Rhodamine B dye by cotton textile coated with SiO_2-TiO_2 and SiO_2-TiO_2-HY composites, J. Photochem. Photobiol., A, 346 (2017) 60–69.
[22] H. Che, G. Che, E. Jiang, C. Liu, H. Dong, C. Li, A novel Z-scheme CdS/Bi_3O_4Cl heterostructure for photocatalytic degradation of antibiotics: mineralization activity, degradation pathways and mechanism insight, J. Taiwan Inst. Chem. Eng., 91 (2018) 224–234.
[23] Y. Ma, X. Zhu, S. Xu, G. He, L. Yao, N. Hu, Y. Su, J. Feng, Y. Zhang, Z. Yang, Gold nanobipyramid@cuprous oxide jujube-like nanostructures for plasmon-enhanced photocatalytic performance, Appl. Catal., B, 234 (2018) 26–36.
[24] X. Li, Y. Ma, Z. Yang, S. Xu, L. Wei, D. Huang, T. Wang, N. Hu, Y. Zhang, Hierarchical heterostructures based on prickly Ni nanowires/Cu_2O nanoparticles with enhanced photocatalytic activity, Dalton Trans., 45 (2016) 7258–7266.
[25] S. Arshadi-Rastabi, J. Moghaddam, M.R. Eskandarian, Synthesis, characterization and stability of Cu_2O nanoparticles produced via supersaturation method considering operational parameters effect, J. Ind. Eng. Chem., 22 (2015) 34–40.
[26] W.-Y. Cheng, T.-H. Yu, K.-J. Chao, S.-Y. Lu, Cu_2O-decorated CdS nanostructures for high efficiency visible light driven hydrogen production, Int. J. Hydrogen Energy, 38 (2013) 9665–9672.
[27] H. Yang, G. Sun, L. Zhang, Y. Zhang, X. Song, J. Yu, S. Ge, Ultrasensitive photoelectrochemical immunoassay based on CdS@Cu_2O co-sensitized porous ZnO nanosheets and promoted by multiwalled carbon nanotubes, Sens. Actuators, B, 234 (2016) 658–666.
[28] L. Wang, W. Wang, Y. Chen, L. Yao, X. Zhao, H. Shi, M. Cao, Y. Liang, Heterogeneous p-n junction CdS/Cu_2O nanorod arrays: synthesis and superior visible-light-driven photoelectrochemical performance for hydrogen evolution, ACS Appl. Mater. Interfaces, 10 (2018) 11652–11662.
[29] N. Qutub, B. Masood Pirzada, K. Umar, S. Sabir, Synthesis of CdS nanoparticles using different sulfide ion precursors: formation mechanism and photocatalytic degradation of Acid Blue-29, J. Environ. Chem. Eng., 4 (2016) 808–817.
[30] Z. Zhang, Y. Ren, L. Han, G. Xie, B. Zhong, Mixed-solvothermal synthesis of CdS micro/nanostructures with optical and ferromagnetic properties, Physica E, 92 (2017) 30–35.
[31] D. Fernando, M. Khan, Y. Vasquez, Control of the crystalline phase and morphology of CdS deposited on microstructured surfaces by chemical bath deposition, Mater. Sci. Semicond. Process., 30 (2015) 174–180.
[32] B.S. Rao, B.R. Kumar, V.R. Reddy, T.S. Rao, Preparation and characterization of CdS nanoparticles by chemical co-precipitation technique, Chalcogenide Lett., 8 (2011) 177–185.
[33] P. Rodrgues, N. Muñoz-Aguirre, E. San-Martin Martínez, G. Gonzalez, O. Zelaya, J. Mendoza, Formation of CdS nanoparticles using starch as capping agent, Appl. Surf. Sci., 255 (2008) 740–742.
[34] R. Borah, E. Saikia, S. Jyoti Bora, B. Chetia, Banana pulp extract mediated synthesis of Cu_2O nanoparticles: an efficient heterogeneous catalyst for the ipso-hydroxylation of arylboronic acids, Tetrahedron Lett., 58 (2017) 1211–1215.
[35] W. Zhang, Y. Ma, Z. Yang, X. Tang, X. Li, G. He, Y. Cheng, Z. Fang, R. He, Y. Zhang, Analysis of synergistic effect between graphene and octahedral cuprous oxide in cuprous oxide-graphene composites and their photocatalytic application, J. Alloys Compd., 712 (2017) 704–713.
[36] M.M.J. Sadiq, A.S. Nesaraj, Reflux condensation synthesis and characterization of Co_3O_4 nanoparticles for photocatalytic applications, Iran. J. Catal., 4 (2014) 219–226.
[37] P. Kubelka, F. Munk, Ein Beitrag zur Optik der Farbanstriche, Zeitschrift für technische Physik, 12 (1931) 593–601.
[38] J. Tauc, R. Grigorovici, A. Vancu, Optical properties and electronic structure of amorphous germanium, Phys. Status Solidi B, 15 (1996) 627–637.
[39] S. Dianat, Visible light induced photocatalytic degradation of direct red 23 and direct brown 166 by $InVO_4$-TiO_2 nanocomposite, Iran. J. Catal., 8 (2018) 121–132.
[40] M. Karimi-Shamsabadi, M. Behpour, A. Kazemi Babaheidari, Z. Saberi, Efficiently enhancing photocatalytic activity of NiO-ZnO doped onto nanozeoliteX by synergistic effects of p-n heterojunction, supporting and zeolite nanoparticles in photo-degradation of Eriochrome Black T and Methyl Orange, J. Photochem. Photobiol., A, 346 (2017) 133–143.
[41] S.G. Ghugal, S.S. Umare, R. Sasikala, A stable, efficient and reusable CdS–SnO_2 heterostructured photocatalyst for the mineralization of Acid Violet 7 dye, Appl. Catal., A, 496 (2015) 25–31.
[42] H. Kisch, H. Weiß, Tuning photoelectrochemical and photocatalytic properties through electronic semiconductor–support interaction, Adv. Funct. Mater., 12 (2002) 483–488.
[43] P. Mohammadyari, A. Nezamzadeh-Ejhieh, Supporting of mixed ZnS–NiS semiconductors onto clinoptilolite nanoparticles to improve its activity in photodegradation of 2-nitrotoluene, RSC Adv., 5 (2015) 75300–75310.
[44] D.-L. Guan, C.-G. Niu, X.-J. Wen, H. Guo, C.-H. Deng, G.-M. Zeng, Enhanced Escherichia coli inactivation and oxytetracycline hydrochloride degradation by a Z-scheme silver iodide decorated bismuth vanadate nanocomposite under visible light irradiation, J. Colloid Interface Sci., 512 (2018) 272–281.
[45] J. Lin, L. Wang, C. Sun, Influence factors and kinetic study on photocatalytic degradation of Rhodamine B by Fe-doped TiO_2/diatomite composite, Adv. Mater. Res., 535–537 (2012) 2209–2213.
[46] G.V. Morales, E.L. Shan, R. Cornejo, E.M. Farfan Torres, Kinetic studies of the photocatalytic degradation of tartrazine, Lat. Am. Appl. Res., 42 (2012) 45–49.
[47] A. Nezamzadeh-Ejhieh, Z. Ghanbari-Mobarakehi, Heterogeneous Photodegradation of 2,4-dichlorophenol using FeO doped onto nano-particles of zeolite P, J. Ind. Eng. Chem., 21 (2015) 668–676.
[48] M. Zarifeh-Alsadat, A. Nezamzadeh-Ejhieh, Removal of phenol content of an industrial wastewater via a heterogeneous photodegradation process using supported FeO onto nanoparticles of Iranian clinoptilolite, Desal. Wat. Treat., 57 (2016) 16483–16494.
[49] S. Dharmraj Khairnar, M. Rajendra Patil, V. Shankar Shrivastava, Hydrothermally synthesized nanocrystalline Nb_2O_5 and its visible-light photocatalytic activity for the degradation of congo red and methylene blue, Iran. J. Catal., 8 (2018) 143–150.
[50] A. Nezamzadeh-Ejhieh, M. Bahrami, Investigation of the photocatalytic activity of supported ZnO-TiO_2 on clinoptilolite nano-particles towards photodegradation of wastewater-contained phenol, Desal. Wat. Treat., 55 (2015) 1096–1104.]
[51] S. Mousavi-Mortazavi, A. Nezamzadeh-Ejhieh, Supported iron oxide onto an Iranian clinoptilolite as a heterogeneous catalyst for photodegradation of furfural in a wastewater sample, Desal. Wat. Treat., 57 (2016) 10802–10814.
[52] P.K. Surolia, R.V. Jasra, Photocatalytic degradation of p-nitrotoluene (PNT) using TiO_2-modified silver-exchanged NaY zeolite: kinetic study and identification of mineralization pathway, Desal. Wat. Treat., 57 (2016) 22081–22098.

[53] D.A. Aljuboury, P. Palaniandy, H.B. Abdul Aziz, S. Feroz, S.S. Abu Amr, Evaluating photo-degradation of COD and TOC in petroleum refinery wastewater by using TiO_2/ZnO photo-catalyst, Water Sci. Technol., 74 (2016) 1312–1325.
[54] A. Khataee, F. Salahpour, M. Fathinia, B. Seyyedi, B. Vahid, Iron rich laterite soil with mesoporous structure for heterogeneous Fenton-like degradation of an azo dye under visible light, J. Ind. Eng. Chem., 26 (2015) 129–135.
[55] A. Nandi, I.B. Chatterjee, Scavenging of superoxide radical by ascorbic acid, J. Biosci., 11 (1987) 435–441.
[56] P. Wardman, Reduction potentials of one-electron couples involving free-radicals in aqueous solution, J. Phys. Chem. Ref. Data, 18 (1989) 1637–1755.
[57] J. De Laat, G. Truong Le, B. Legube, A comparative study of the effects of chloride, sulfate, and nitrate ions on the rates of decomposition of H_2O_2 and organic compounds by Fe(II)/H_2O_2 and Fe(III)/H_2O_2, Chemosphere, 55 (2004) 715–723.
[58] D.A. Armstronga, R.E. Huie, S. Lymar, W.H. Koppenol, G. Merényi, P. Neta, D.M. Stanbury, S. Steenken, P. Wardman, Standard electrode potentials involving radicals in aqueous solution: inorganic radicals, Bioinorg. React. Mech., 9 (2013) 59–61.
[59] B.A. Wols, C.H.M. Hofman-Caris, Review of photochemical reaction constants of organic micropollutants required for UV advanced oxidation processes in water, Water Res., 46 (2012) 2815–2827.
[60] G.V. Buxton, C.L. Greenstock, W.P. Helman, A.B. Ross, Critical review of rate constants for reactions of hydrated electrons, hydrogen atoms and hydroxyl radicals ($^{\bullet}OH/^{\bullet}O^{-}$) in aqueous solution, J. Phys. Chem. Ref. Data, 17 (1988) 513–886.
[61] R.M. Buoro, V.C. Diculescu, I.C. Lopes, S.H.P. Serrano, A.M. Oliveira-Brett, Electrochemical oxidation of sulfasalazine at a glassy carbon electrode, Electroanalysis, 26 (2014) 924–930.